Molecular Mechanics Calculation of Inner-Shell Activation Barriers to Heterogeneous Electron Transfer in $M(tacn)_2^{3+/2+}$ Redox Couples (M = Fe, Co, Ni; tacn = 1,4,7-Triazacyclononane)

Ying-Duo Gao, Kenny B. Lipkowitz,* and Franklin A. Schultz*

Contribution from the Department of Chemistry, Indiana University−Purdue University at Indianapolis, 402 North Blackford Street, Indianapolis, Indiana 46202-3274

Received January 18, 1995[⊗]

Abstract: $M(tacn)_2^{3+/2+}$ redox couples (M = Fe, Ni, Co; tacn = 1,4,7-triazacyclononane) exhibit different extents of M−N bond lengthening upon electrochemical reduction and standard heterogeneous rate constants ($k_{s,h}$) that decrease systematically in accord with this structural feature. Inner-shell enthalpies of activation ($\Delta H^{\ddagger}_{is}$) obtained from temperature-dependent measurements of $k_{s,h}$ [Crawford, P. W.; Schultz, F. A. *Inorg. Chem.* **1994**, *33*, 4344] equal 1.7, 1.9, and 13.2 kcal mol^{-1} for M = Fe, Ni, and Co, respectively, in contrast with values of 0.2, 2.2, and 6.0 kcal mol^{-1} calculated by the harmonic oscillator model of M−N bond elongation. In an attempt to resolve this discrepancy we have carried out molecular mechanics calculation of $\Delta H^{\ddagger}_{is}$ for $M(tacn)_2^{3+/2+}$ couples using MMX and CHARMM force fields. The procedure for doing so involves intersecting potential energy curves of oxidized and reduced reactants generated from the force field parameters required to optimize the ground state structure of each oxidation state. MMX barrier heights estimated in this way are in close correspondence with the harmonic oscillator approximation widely used in Marcus theory calculation of inner-shell reorganization energies. The vibrational entropies of the molecules are calculated, and differences in these quantities correlate with the half-reaction entropy ($\Delta S°_{rc}$) of the $M(tacn)_2^{3+/2+}$ couples. Non-zero, metal-dependent values of $\Delta S°_{rc}$ for these complexes are thought to arise from changes in M−N frequencies upon reduction [Richardson, D. E.; Sharpe, P. *Inorg. Chem.* **1991**, *30*, 1412]. Poor correspondence between measured and calculated activation enthalpies remains in cases where the electrode reaction exhibits a large half-reaction entropy. The molecular mechanics force fields are used to partition the energy of the molecules into component terms, and it is found that the majority of the inner-shell barrier derives from M−N bond stretching.

Introduction

A current focus in electron transfer chemistry is the correlation between molecular structure and the rate of electron transfer predicted by Marcus theory.[1] One component of the barrier to such processes is the inner-shell energy of activation, which arises from structural differences between reactants and products and can limit the rate of electron transfer if large changes in coordinates accompany a change in oxidation state. In an effort to illustrate this expectation, one of us[2] recently measured heterogeneous electron transfer rates and activation parameters for a series of $M(tacn)_2^{3+}$ complexes (M = Fe, Co, Ni, Ru; tacn = 1,4,7-triazacyclononane, Chart 1)[3] whose electrochemical reduction

$$M(tacn)_2^{3+} + e^- \rightleftharpoons M(tacn)_2^{2+} \qquad (1)$$

is accompanied by different extents of M−N bond lengthening (Table 1). Although room temperature electrochemical rate constants ($k_{s,h}$) for reaction 1 correlate closely with inner-shell barriers calculated from a harmonic oscillator model for the change in M−N bond distance [$(\Delta H^{\ddagger}_{is})_{HO}$], experimental inner-shell enthalpies of activation [$(\Delta H^{\ddagger}_{is})_{exp}$] obtained from the temperature dependence of $k_{s,h}$ do not.

However, internal degrees of freedom other than the change in M−N bond distance may contribute to $\Delta H^{\ddagger}_{is}$, particularly for complexes containing the structurally complex tacn ligand. Thus, we sought a more rigorous method of estimating inner-shell reorganization energies to better understand reasons for the discrepancy between $(\Delta H^{\ddagger}_{is})_{exp}$ and $(\Delta H^{\ddagger}_{is})_{HO}$. This paper describes calculation of the inner-shell enthalpies of activation of $M(tacn)_2^{3+/2+}$ redox couples by molecular mechanics. The work includes the development of force field parameters appropriate to each metal in both oxidation states and calculation

Chart 1. Ligand Structures and Abbreviations

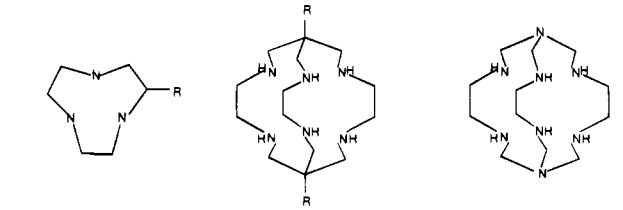

[⊗] Abstract published in *Advance ACS Abstracts*, November 15, 1995.

(1) (a) Marcus, R. A. *J. Chem. Phys.* **1956**, *24*, 966. (b) Marcus, R. A. *J. Chem. Phys.* **1965**, *43*, 679. (c) Marcus, R. A. *Electrochim. Acta* **1968**, *13*, 995.

(2) Crawford, P. W.; Schultz, F. A. *Inorg. Chem.* **1994**, *33*, 4344.

(3) Ligand names and abbreviations (see Chart 1): en = 1,2-ethanediamine; tacn = 1,4,7-triazacyclononane; Metacn = 2-methyl-1,4,7-triazacyclononane; sar = 3,6,10,13,16,19-hexaazabicyclo[6.6.6]eicosane; $(NO_2)_2$(sar) = 1,8-dinitro-3,6,10,13,16,19-hexaazabicyclo[6.6.6]eicosane; $[(NH_2OH)_2(sar)]^{2+}$ = 1,8-bis(hydroxyamino)-3,6,10,13,16,19-hexaazabicyclo-[6.6.6]eicosane; $[(NH_3)_2(sar)]^{2+}$ = 1,8-diammonio-3,6,10,13,16,19-hexaazabicyclo[6.6.6]eicosane; sep = sepulchrate = 1,3,6,8,10,13,16,19-octaazabicyclo[6.6.6]eicosane.

0002-7863/95/1517-11932$09.00/0

Table 1. Metal−Nitrogen Bond Distances, Electrochemical Rate Constants, and Inner-Shell Enthalpies of Activation of $M(tacn)_2^{3+/2+}$ Complexes

metal	M^{III}−N, Å	M^{II}−N, Å	Δr, Å	$k_{s,h}$,[a] cm s^{-1}	$(\Delta H^{\ddagger}_{is})_{exp}$,[b] kcal mol^{-1}	$(\Delta H^{\ddagger}_{is})_{HO}$,[c] kcal mol^{-1}
Fe	1.99	2.03	0.04	0.8	1.7	0.2
Ni	1.971(4), 2.109(2)[d]	2.105	0.134, 0.004	0.12	1.9	2.2
Co	1.974	2.155	0.181	0.016	13.2	6.0

[a] Double-layer corrected standard heterogeneous rate constant measured at 25 °C in NaF electrolyte. [b] Experimental inner-shell enthalpy of activation determined from the temperature dependence of $k_{s,h}$ in 0.75 M NaF and subtraction of an outer-shell contribution of 3.5 kcal mol^{-1} for each couple (from ref 2). [c] Calculated from eq 4 using the tabulated changes in M−N bond distance and a reduced force constant of 1.70 mdyn Å^{-1}. [d] The $Ni(tacn)_2^{3+}$ complex is Jahn−Teller distorted in the solid state and has four short and two long M−N bonds.

of optimized structures based on these parameters. An assessment of the relative contributions of various deformational motions to $\Delta H^{\ddagger}_{is}$ is made based on full force field treatments which consider all atomic interactions in the molecules rather than only the M−N bond lengthenings. Estimation of inner-shell barrier heights is achieved by intersecting potential energy curves generated from optimized reactant and product structures. Inner-shell enthalpies of activation estimated in this way are compared with experimental values and with those obtained from the harmonic oscillator model. It is found that calculated and experimental barrier heights show poor agreement in cases where the electrode reaction has a large half-reaction entropy, ΔS°_{rc}.

Experimental Section

Molecular Mechanics Calculations. Molecular mechanics calculations were carried out with the MMX force field implemented in PCMODEL 4.0 obtained from Serena Software, Inc. and with the CHARMM force field obtained from MSI, Inc. Parameter sets for these force fields were developed by minimizing the root mean square (rms) deviation between computed atom coordinates and those obtained from X-ray crystal structures of isolated compounds. The potential energy functions used in the MMX and CHARMM force fields are given in Chart 2. In carrying out minimizations with MMX only the stretching, bending, torsion, and van der Waals terms were applied to metal atoms; all six energy terms were applied to the remaining atoms in the structure. All energy functions except the improper torsion term were used throughout in calculations with CHARMM. The standard block-diagonal Newton−Raphson optimizer was used in PCMODEL. The adopted basis Newton−Raphson optimizer followed by the Newton−Raphson optimizer were used in CHARMM to ensure that the optimized geometries were true minima rather than saddle points on the potential energy surface. In all cases the dielectric constant of the medium was set equal to 1.0 and extended cutoffs (see Chart 2) were used. Calculation of vibrational entropy was done with the CHARMM Vibran routine.

Estimation of Reorganization Energies. Inner-shell reorganization energies are estimated by overlaying the potential energy curves of the $M(tacn)_2^{3+}$ reactants and $M(tacn)_2^{2+}$ products as each is distorted into the geometry of the other. To assess the extent to which various degrees of freedom contribute to these barriers, input geometries and subsequent calculations were enacted with the **Z**-matrix formalism,[4] which defines the coordinates of all atoms in a molecule. For calculation of reorganization energies a pair of molecules is used to define initial and final **Z**-matrices; these correspond to the geometries of the energy-minimized $M(tacn)_2^{3+}$ and $M(tacn)_2^{2+}$ structures. Then, each element of the initial **Z**-matrix is incrementally adjusted to the final value, and the internal energy of the molecule is calculated at each step along the way. The number of increments, n, between initial and final structures was set equal to 10. Finer discretization was tested in several cases and gave similar results. All values reported here were calculated with $n = 10$. The assumption is made that all degrees of freedom change proportionately throughout the reaction coordinate. While this is not strictly true, it is anticipated that the differences are small and do not affect results significantly.

Chart 2. Potential Energy Functions in MMX and CHARMM Force Fields

MMX

$$E_{total} = \Sigma (E_s + E_b + E_{tor} + E_{vdw} + E_{s\text{-}b} + E_{d\text{-}d})$$

Stretching

$$E_s = 143.88 \cdot 1/2 \cdot k_s \cdot (1 - 2.000 \cdot (r - r_o)) \cdot (r - r_o)^2$$

Bending

$$E_b = 0.043828 \cdot 1/2 \cdot k_b \cdot (\theta - \theta_o)^2 \cdot (1 + 7.0 \times 10^{-7} \cdot (\theta - \theta_o)^4)$$

Torsion

$$E_{tor} = 1/2 \cdot V_1 \cdot (1 + \cos \omega) + 1/2 \cdot V_2 \cdot (1 - \cos 2\omega) + 1/2 \cdot V_3 \cdot (1 + \cos 3\omega)$$

Van der Waals

$$E_{vdw} = \varepsilon \cdot 290{,}000 \cdot \exp^{-12.5/p} - 2.25 \cdot p^6 \qquad p = (r_i - r_k)/r_o < 3.311)$$

$$E_{vdw} = \varepsilon \cdot 336.17 \cdot p^2 \qquad p = (r_i - r_k)/r_o > 3.311)$$

Stretch-Bend

$$E_{s\text{-}b} = k_{s\text{-}b} \cdot (\theta - \theta_o) \cdot (r_1 - r_{10} + r_2 - r_{20})$$

$k_{s\text{-}b}$ = 0.120 (X-F-Y), 0.250 (X-S-Y), 0.090 (X-F-H) -0.40 (X-S-H)

where F and S are 1st and 2nd row elements, respectively, X and Y are any 1st or 2nd row elements and H is hydrogen

Dipole-Dipole

$$E_{d\text{-}d} = B_{mom(i,k)} \cdot B_{mom(m,n)} \cdot (\cos x - 3 \cos A \cdot \cos B)/(1.5 \cdot r^3)$$

CHARMM

$$E_{total} = \Sigma (E_s + E_b + E_{tor} + E_{\omega} + E_{vdw} + E_{el})$$

Stretching

$$E_s = k_s \cdot (r - r_o)^2$$

Bending

$$E_b = k_b \cdot (\theta - \theta_o)^2$$

Torsion

$$E_{tor} = k_{\phi} - k_{\phi} \cdot \cos(n\phi)$$

Improper Torsion

$$E_{\omega} = S\, k_{\omega} \cdot (\omega - \omega_o)^2$$

Van der Waals

$$E_{vdw} = A \cdot r_{ij}^{-12} - B \cdot r_{ij}^{-6}$$

Electrostatic

$$E_{el} = S\, (\varepsilon_1 \cdot \varepsilon_2 / 4p\varepsilon_o r_{ij}) \cdot [1 - (r_{ij}/r_{cut})^2]^2$$

$\varepsilon_o = 1.0$ $\quad r_{cut} = 15.0$ Å

Crystal Structures. Experimental coordinates of complexes containing the tacn and sarcophagine ligands[3] were taken from X-ray crystal structures of the following compounds identified by search of the Cambridge Structural Database: $[Fe(tacn)_2]Cl_2 \cdot 4H_2O$,[5] $[Fe(tacn)_2]Cl_3 \cdot 5H_2O$,[5] $[Ni(tacn)_2](NO_3)Cl \cdot H_2O$,[6] $[Ni(tacn)_2]_2(S_2O_6)_3 \cdot 7H_2O$,[7] $[Co(tacn)_2]$-

(4) Clark, T. *A Handbook of Computational Chemistry: A Practical Guide to Chemical Structure and Energy Calculations*; Wiley: New York, 1985; Chapter 3.3.

(5) Boeyens, J. C. A.; Forbes, A. G. S.; Hancock, R. D.; Wieghardt, K. *Inorg. Chem.* **1985**, *24*, 2926.

(6) Zompa, L. J.; Margulis, T. N. *Inorg. Chim. Acta* **1978**, *28*, L157.

$I_2 \cdot 2H_2O$,[8] $[Co((NO_2)_2sar\text{-}H)]Cl_2 \cdot 4H_2O$,[9] $[Co((NH_2OH)_2sar)]Cl_5 \cdot 4H_2O$,[10] and $[Ni((NH_3)_2sar)](NO_3)_4 \cdot H_2O$.[11] No crystal structure of $Co(tacn)_2^{3+}$ exists. Therefore, the structure of $[Co((R)\text{-Metacn})_2]I_3 \cdot 5H_2O$[12] was used in its place. Although this crystal is disordered (methyl groups appear to be present on all six carbon atoms of each tacn ring), its structure provides a valid Co(III)−N distance (1.974 Å) for force field parametrization.

Results and Discussion

Computational Methods. At the outset of this research we explored the use of *ab initio* and semiempirical quantum mechanical methods for calculation of metal complex structures.[13] However, *ab initio* calculations proved to be too time consuming,[14] and semiempirical methods were not able to replicate structures accurately. Calculations with ZINDO and AMPAC consistently overestimated M−N bond distances and often predicted pentacoordination. Based on the inability of these methods to reproduce ground state structures, we turned to molecular mechanics for investigation of metal complexes.

Molecular mechanics is a non-quantum mechanical method for computing structures, energies, and some properties of molecules. It consists of an empirical force field which is a collection of functions and parameters that define the potential energy associated with stretching, bending, torsion, and other interactions in a molecule. Its use in organic chemistry has been widespread for many years,[15] and applications in inorganic chemistry are becoming more frequent.[16] Early work focused almost solely on Co(III) amines,[17] but more recently force field parametrization has been extended to a wider range of coordination compounds[18] and to metallocenes.[19] A number of molecular mechanics programs are suitable for modeling transition metal complexes. The two we have chosen are MMX, which is an extended version of Allinger's MM2 force field, and CHARMM. Although both are valence force fields, they have been developed independently from different experimental data and hence differ in the number, form, and parameters of their potential energy functions as indicated in Chart 2. It is important to implement two unrelated force fields, because use of more than one provides confidence in the final results, if these prove to be the same.

Energy Minimization and Force Field Parametrization. Energy minimized structures of the $M(tacn)_2^{3+}$ and $M(tacn)_2^{2+}$ complexes were determined for M = Fe, Ni, and Co. The parameters found to have the greatest influence on structure optimization were the stretching force constants (k_s) and strain-free distances (r_0) of the M−N bonds and the bending force constants (k_b) and strain-free values (θ_0) of the M−N−C and M−N−H angles. Optimized values of these parameters for MMX and CHARMM are presented in Table 2. The remaining terms in the parameter sets are available from the authors upon request. The computed metal−nitrogen bond distances and heavy atom rms deviations of the energy minimized structures are compared with X-ray structures in Table 3. The latter data indicate that both MMX and CHARMM accurately reproduce the structures of $M(tacn)_2^{3+}$ and $M(tacn)_2^{2+}$. CHARMM is slightly superior based on rms values. Figure 1 illustrates the goodness of fit between experimental and MMX-calculated structures of $Co(tacn)_2^{2+}$. Also, it should be noted that both MMX and CHARMM accurately treat the static Jahn−Teller distortion in $Ni(tacn)_2^{3+}$. This is accomplished by identifying two types of nitrogens in the $Ni(tacn)_2^{3+}$ structure and assigning to each a unique set of parameters to reproduce the distorted crystal geometry.

The numerical values of the optimized parameters of the two force fields are different, as expected. As shown in Table 2, MMX values of k_s are more sensitive to the metal oxidation state than are those of CHARMM, whereas CHARMM gives values of r_0(M−N) that are larger and closer to X-ray crystallographic distances. Also, the strain-free M−N−C and M−N−H bond angles in CHARMM are ≈120°, whereas these are closer to tetrahedral values in MMX. For both force fields, angle-bending force constants are about an order of magnitude smaller than bond-stretching force constants.

The values of k_s(M−N) and r_0(M−N) obtained by MMX for Fe(III), Ni(II), Co(III), and Co(II) are similar numerically to those reported by other workers using comparable valence force fields.[16c,18,20] Values of bond-stretching force constants and strain-free distances for Ni(III)−N and low-spin Fe(II)−N are reported here for the first time. Although molecular mechanics force field parameters differ fundamentally from force constants derived from vibrational spectroscopic data, it is interesting to note that a close numerical correlation exists between the values of k_s(M−N) obtained by MMX in Table 2 and the M−N stretching force constants derived from a GVFF analysis of skeletal IR and Raman data of transition metal−ammine complexes.[21] In both instances, values of $k_s \approx 1.7$ and 0.9 mdyn Å^{-1} are observed for tri- and divalent first-row transition elements, respectively. Müller finds stretching force constants

(7) Wieghardt, K.; Walz, W.; Nuber, B.; Weiss, J.; Ozarowski, A.; Stratemeier, H.; Reinen, D. *Inorg. Chem.* **1986**, *25*, 1650.

(8) Kuppers, H.-J.; Neves, A.; Pomp, C.; Ventur, D.; Wieghardt, K.; Nuber, B.; Weiss, J. *Inorg. Chem.* **1986**, *25*, 2400.

(9) Geue, R. J.; Hambley, T. W.; Harrowfield, J. M.; Sargeson, A. M.; Snow, M. R. *J. Am. Chem. Soc.* **1984**, *106*, 5478.

(10) Balahura, R. J.; Ferguson, G.; Ruhl, B. L.; Wilkins, R. G. *Inorg. Chem.* **1983**, *22*, 3990.

(11) Clark, I. J.; Creaser, I. I.; Engelhardt, L. M.; Harrowfield, J. M.; Krausz, E. R.; Moran, G. M.; Sargeson, A. M.; White, A. H. *Aust. J. Chem.* **1993**, *46*, 111.

(12) Mikami, M.; Kuroda, R.; Konno, M.; Saito, Y. *Acta Crystallogr.* **1977**, *B33*, 1485.

(13) *Ab initio* calculations were carried out with Gaussian-92 (Gaussian, Inc., Carnegie Office Park, Building 6, Pittsburgh, PA 15106) on a Cray supercomputer. Semiempirical calculations were carried out using the SAM1 hamiltonian in AMPAC (Semichem, 12716 West 66th Terrace, Shawnee, KS 66216) and the INDO hamiltonian in ZINDO (BIOSYM Technologies Inc., 9685 Scranton Road, San Diego, CA 92121). In all cases, appropriate charges and spin states were assigned to the cationic complexes. Anionic counterions and solvent molecules were not included in the calculations. All default parameters and settings were used throughout. In two instances (Ni^{2+} and Fe^{3+}) SCF convergence could not be achieved with ZINDO unless alternative convergence routines were implemented. For all complexes, several different starting geometries including the X-ray structure were used for the optimization. The Newton−Raphson optimizer with analytic Hessian, calculated with a first-order approximation search method, was used for ZINDO. ZINDO is parametrized for Fe, Co, and Ni, while AMPAC has only a preliminary set of parameters for Fe.

(14) For example, calculations on a Cray 2 employing Gaussian 92 with 132 primitive functions to describe $Fe(tacn)_2^{2+}$ did not converge after 28 cpu hours.

(15) (a) Burkert, U.; Allinger, N. L. *Molecular Mechanics*; Monograph 177; American Chemical Society: Washington, DC, 1982; p 86. (b) Bowen, J. P.; Allinger, N. L. In *Reviews in Computational Chemistry*; Lipkowitz, K. B., Boyd, D. B., Eds.; VCH Publishers, Inc.: New York, 1991; Vol. 2, Chapter 3. (c) Dinur, U.; Hagler, A. T. ref 15b, Chapter 4.

(16) (a) Brubaker, G. R.; Johnson, D. W. *Coord. Chem. Rev.* **1984**, *53*, 1. (b) Hancock, R. D. *Progr. Inorg. Chem.* **1989**, *36*, 187. (c) Comba, P. *Coord. Chem. Rev.* **1993**, *123*, 1. (d) Landis, C. R.; Root, D. M.; Cleveland, T. In *Reviews in Computational Chemistry*; Lipkowitz, K. B., Boyd, D. B., Eds.; VCH Publishers, Inc.: New York, 1995; Vol. 6, Chapter 2.

(17) (a) Corey, E. J.; Bailar, J. C. *J. Am. Chem. Soc.* **1959**, *81*, 2620. (b) Snow, M. R. *J. Am. Chem. Soc.* **1970**, *92*, 3610. (c) DeHayes, L. J.; Busch, D. H. *Inorg. Chem.* **1973**, *12*, 1505.

(18) Bernhardt, P. V.; Comba, P. *Inorg. Chem.* **1992**, *31*, 2638.

(19) Doman, T. N.; Landis, C. R.; Bosnich, B. *J. Am. Chem. Soc.* **1992**, *114*, 7264.

(20) (a) Bond, A. M.; Hambley, T. W.; Snow, M. R. *Inorg. Chem.* **1985**, *24*, 1920. (b) Yoshikawa, Y. *J. Comput. Chem.* **1990**, *11*, 326.

(21) (a) Schmidt, K. H.; Müller, A. *Inorg. Chem.* **1975**, *14*, 2183. (b) Schmidt, K. H.; Müller, A. *Coord. Chem. Rev.* **1976**, *19*, 41.

Table 2. Empirical Force Field Parameters for $M(tacn)_2^{3+/2+}$ Complexes

M	k_s(M−N), mdyn Å^{-1}	r_0(M−N), Å	k_b(M−N−C), mdyn Å rad^{-2}	θ_0(M−N−C), deg	k_b(M−N−H), mdyn Å rad^{-2}	θ_0(M−N−H), deg
			MMX			
Fe^{3+}	1.75	1.92	0.20	109.5	0.10	107.7
Fe^{2+}	1.40	1.94	0.20	109.5	0.10	107.7
Ni^{3+}	1.75	1.930	0.20	109.0	0.10	104.0
	1.75	2.090	0.20	105.0	0.10	102.0
Ni^{2+}	0.90	2.080	0.20	105.0	0.10	102.0
Co^{3+}	1.75	1.908	0.20	109.5	0.10	109.5
Co^{2+}	1.00	2.130	0.20	109.5	0.10	109.5
			CHARMM			
Fe^{3+}	1.50	2.000	0.14	121.0	0.14	112.5
Fe^{2+}	1.39	2.031	0.14	120.0	0.07	112.5
Ni^{3+}	1.53	1.968	0.14	117.0	0.14	113.0
	1.39	2.112	0.14	112.5	0.14	113.0
Ni^{2+}	1.39	2.115	0.14	114.8	0.14	112.0
Co^{3+}	1.50	1.973	0.14	115.0	0.07	112.5
Co^{2+}	1.25	2.156	0.14	114.0	0.07	112.5

Table 3. Actual and Calculated Metal−Nitrogen Bond Distances of $M(tacn)_2^{3+/2+}$ Complexes

		MMX		CHARMM	
M	r(M−N)$_{X\text{-}ray}$, Å	r(M−N)$_{calc}$, Å	rms, Å	r(M−N)$_{calc}$, Å	rms, Å
Fe^{3+}	1.99	2.00	0.046	2.00	0.030
Fe^{2+}	2.03	2.03	0.059	2.03	0.036
Ni^{3+}	2.109	2.110	0.070	2.110	0.054
	1.971	1.980		1.970	
Ni^{2+}	2.105	2.110	0.070	2.110	0.039
Co^{3+}	1.974	1.975		1.975	
Co^{2+}	2.155	2.150	0.052	2.150	0.038

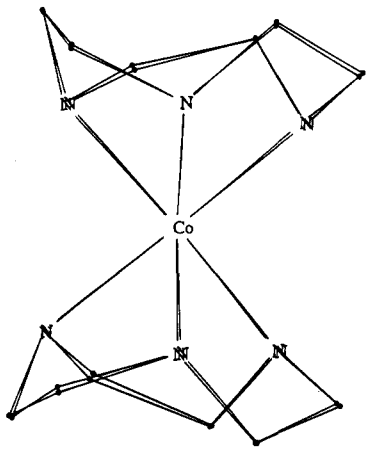

Figure 1. Experimental and MMX-calculated structures of $Co(tacn)_2^{2+}$.

to be somewhat independent of metal and larger values of k_s (stiffer restoring force) for M^{3+} compared with M^{2+}, as anticipated. Generally, our parameters parallel these trends. The MMX result k_s(M−N) = 1.4 mdyn Å^{-1} for $Fe(tacn)_2^{2+}$ (Table 2) is noteworthy in that it is larger than the value for other divalent elements and therefore consistent with the characterization of the metal atom in this complex[5] as low-spin Fe(II).

Parametrization of molecular mechanics force fields is done so that structures and properties of molecules can be computed with accuracy. One way to evaluate the validity of a parameter set is to use results derived from one group of compounds to predict the structures of a second group. This is an important comparison to make in the present work, because limited structural information is available for parameter development. Therefore, we used the parameters obtained from the $M(tacn)_2^{3+}$ and $M(tacn)_2^{2+}$ calculations to compute the structures of three metal−sarcophagine complexes whose experimental geometries

Table 4. Actual, Calculated, and Strain-Free Metal−Nitrogen Bond Distances of Cobalt(III) and Nickel(II) Sarcophagine Complexes

		original parameters			adjusted parameters		
	$r_{X\text{-}ray}$, Å	r_0, Å	r_{calc}, Å	rms, Å	r_0, Å	r_{calc}, Å	rms, Å
			MMX				
$Co((NO_2)_2sar\text{-}H)^{2+}$	1.976	1.908	1.963	0.18	1.928	1.974	0.16
$Co((NH_2OH)_2sar)^{5+}$	1.973	1.908	1.963	0.09	1.935	1.978	0.09
$Ni((NH_3)_2sar)^{4+}$	2.109	2.080	2.180	0.23	2.050	2.120	0.28
			CHARMM				
$Co((NO_2)_2sar\text{-}H)^{2+}$	1.976	1.973	1.965	0.19	1.985	1.940	0.14
$Co((NH_2OH)_2sar)^{5+}$	1.973	1.973	1.962	0.12	1.985	1.970	0.08
$Ni((NH_3)_2sar)^{4+}$	2.109	2.115	2.120	0.26	2.115	2.120	0.26

could be retrieved from the Cambridge Structural Database. Table 4 compares their calculated and actual metal−nitrogen bond distances and lists the rms deviations between computed and observed geometries.

Although tacn and sar share many similarities there are important differences between complexes of these ligands. First, the additional hydrocarbon framework of sar results in the formation of five- and six-membered chelate rings, whereas only five-membered rings are present in complexes with tacn. Also, nonbonded repulsions between adjacent tacn ligands[22] are absent when a metal ion is encapsulated by a single sarcophagine molecule. Despite these differences, relatively good agreement is achieved indicating that the force field parameters are transferable. MMX computes a M−N bond distance that is too long in $Ni((NH_3)_2sar)^{4+}$. Adjustment of the strain-free Ni(II)−N distance results in a significant improvement in this value. In fact, adjustment of r_0 in all parameter sets results in some improvement in rms values, as shown in the last three columns of Table 4. However, relatively large rms deviations remain for $Co((NO_2)_2sar\text{-}H)^{2+}$ and $Ni((NH_3)_2sar)^{4+}$. In the former case, a large range of Co(III)−N distances is observed experimentally because one of the secondary nitrogen atoms in the ligand is deprotonated. In the latter case, the complex is distorted in the crystal. Its N−Ni−N angles are 168−170° compared with 178−180° for the other M−sar complexes, and this distortion is not reproduced by the molecular mechanics calculations.

A further means of evaluating the quality of force field parameters is to compute the normal mode frequencies of the molecules for comparison with experiment. Unfortunately, normal mode analyses of the complexes investigated here do

(22) Thöm, V. J.; Boeyens, J. C. A.; McDougall, G. J.; Hancock, R. D. *J. Am. Chem. Soc.* **1984**, *106*, 3198.

Table 5. Calculated and Measured Half-Reaction Entropies of $M(tacn)_2^{3+/2+}$ Redox Couples

M	$\Delta S°_{calc}$,[a] cal mol^{-1} K^{-1}	$\Delta S°_{rc}$,[b] cal mol^{-1} K^{-1}
Fe	1.6	2.6
Ni	5.3	4.3
Co	9.9	22.7

[a] Calculated by CHARMM. [b] Measured in 0.75 M NaF, ref 2.

not exist, so a direct comparison with vibrational spectra cannot be made. However, vibrational partition functions can be determined from the computed normal mode frequencies, and from these the vibrational entropies of the molecules can be calculated. This was done for the three pairs of $M(tacn)_2^{3+/2+}$ complexes, and the differences in entropy between the 3+ and 2+ oxidation states are listed in Table 5 as $\Delta S°_{calc}$. Also listed in Table 5 are values of the half-reaction entropy, $\Delta S°_{rc}$, determined from the temperature dependence of the formal potential of reaction 1.[2] The calculated values of ΔS are positive, reflecting a decrease in normal mode frequency upon reduction. These $\Delta S°_{calc}$ quantities predict the correct trend in entropy change, but in two cases are smaller than $\Delta S°_{rc}$. However, the computed entropy differences are based solely on the vibrational components of the molecules, whereas experimental differences include contributions from solvent and other factors.[23,24]

In summary, the validity of the empirical force field parameters is confirmed by (1) the quality of equilibrium geometries calculated for metal−tacn complexes, (2) the quality of equilibrium geometries calculated for metal−sar complexes, and (3) prediction of the correct trend in entropy changes for the $M(tacn)_2^{3+/2+}$ couples.

Calculation of Inner-Shell Reorganization Energies. The rate constant of a heterogeneous electron transfer reaction can be expressed in terms of molecular features by eq 2:

$$k_{s,h} = A \exp[-(\Delta G^{\ddagger}_{is} + \Delta G^{\ddagger}_{os})/RT] \qquad (2)$$

Here, A is a pre-exponential factor and $\Delta G^{\ddagger}_{is}$ and $\Delta G^{\ddagger}_{os}$ are the inner- and outer-shell free energies of activation, respectively. Because the size, charge, and stoichiometry of the $M(tacn)_2^{3+/2+}$ couples are similar, their pre-exponential factors and outer-shell free energies of activation should be nearly equal. Thus, differences in $k_{s,h}$ originate in $\Delta G^{\ddagger}_{is}$.

Inner-shell contributions to the activation of heterogeneous electron transfer are modeled by overlapping parabolas as shown in Figure 2. The parabolas represent the energies required to distort the nuclei from their equilibrium positions in each oxidation state. Marcus theory is expressed in terms of reorganization energies, the inner-shell part of which equals the energy of the 2+ product in the geometry of the 3+ reactant ($\lambda_{is,2}$) or the energy of the 3+ reactant in the geometry of the 2+ product ($\lambda_{is,3}$). If the force constants for molecular deformations in the two oxidation states are equal, the parabolas have equal curvatures ($\lambda_{is} = \lambda_{is,2} = \lambda_{is,3}$) and the inner-shell contribution to the barrier for thermal electron transfer is given by the energy at the point where the parabolas cross, $\lambda_{is}/4$. Free energy is the variable in eq 2, whereas molecular mechanics calculations provide enthalpies. However, entropic contributions to the activation process usually are neglected, and it is assumed that $\Delta H^{\ddagger}_{is} \cong \Delta G^{\ddagger}_{is} = \lambda_{is}/4$.

Figure 3 illustrates the computational approach for estimating the inner-shell enthalpy of activation. In this procedure the

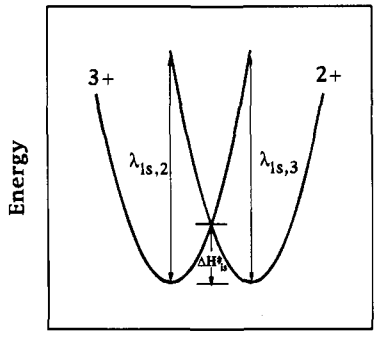

Figure 2. Overlap of the inner-shell component of $M(tacn)_2^{3+}$ and $M(tacn)_2^{2+}$ potential energy curves.

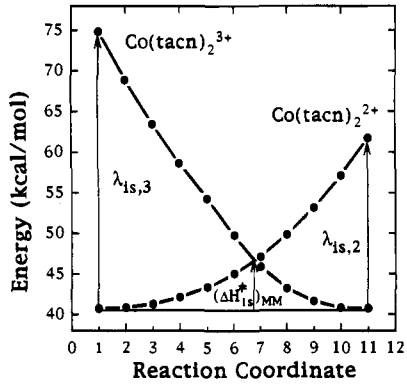

Figure 3. Procedure for estimation of inner-shell enthalpy of activation, $(\Delta H^{\ddagger}_{is})_{MM}$, by overlap of potential energy curves. Results shown are for $Co(tacn)_2^{3+/2+}$ as calculated by MMX.

energy of the $M(tacn)_2^{3+}$ reactant is calculated as it is changed from its equilibrium geometry into that of the $M(tacn)_2^{2+}$ complex using the energy minimized parameters for the 3+ oxidation state (Table 2). Likewise, the energy of the $M(tacn)_2^{2+}$ complex is calculated as it is mutated into the $M(tacn)_2^{3+}$ structure using the parameters for the 2+ oxidation state. The two curves are displaced horizontally from one another by a distance representing the difference in all internal coordinates between initial and final states, and the energy of each oxidation state is calculated at 10% intervals along this coordinate by use of the Z-matrix procedure described in the Experimental Section. The parabolas calculated for the $Co(tacn)_2^{3+/2+}$ couple by MMX are shown in Figure 3 as an example. The inner-shell contribution to the activation barrier is taken as the value of the enthalpy at the point where the two curves cross, $(\Delta H^{\ddagger}_{is})_{MM}$. Alternatively, since the two parabolas have unequal curvatures, the inner-shell contribution may be calculated from reorganization energies according to eq 3 where $\gamma = \lambda_{is,2}/\lambda_{is,3}$:

$$(\Delta H^{\ddagger}_{is})_{reorg} = \frac{\lambda_{is,2}}{(1 + \gamma^{1/2})^2} \qquad (3)$$

Table 6 contains the inner-shell reorganization energies and enthalpies of activation determined by these procedures for each redox couple. The results are compared with values obtained experimentally $[(\Delta H^{\ddagger}_{is})_{exp}]$ and with those calculated from the simple harmonic oscillator expression:

$$(\Delta H^{\ddagger}_{is})_{HO} = 0.5 \sum f_i (\Delta r/2)^2 \qquad (4)$$

where Δr is the change in M−N bond distance and f_i is the reduced force constant which is set equal to 1.7 mdyn Å^{-1}. We note first that values of $(\Delta H^{\ddagger}_{is})_{MM}$ and $(\Delta H^{\ddagger}_{is})_{reorg}$ are in close

(23) Hupp, J. T.; Weaver, M. J. *Inorg. Chem.* **1984**, *23*, 3639.
(24) (a) Richardson, D. E.; Sharpe, P. *Inorg. Chem.* **1991**, *30*, 1412. (b) Richardson, D. E.; Sharpe, P. *Inorg. Chem.* **1993**, *32*, 1809.

Table 6. Inner-Shell Reorganization Energies and Enthalpies of Activation (in kcal mol^{-1}) of M(tacn)$_2^{3+/2+}$ Couples

	MMX				CHARMM					
M	$\lambda_{is,2}$	$\lambda_{is,3}$	$(\Delta H^{\ddagger}_{is})_{MM}$[a]	$(\Delta H^{\ddagger}_{is})_{reorg}$[b]	$\lambda_{is,2}$	$\lambda_{is,3}$	$(\Delta H^{\ddagger}_{is})_{MM}$[a]	$(\Delta H^{\ddagger}_{is})_{reorg}$[b]	$(\Delta H^{\ddagger}_{is})_{HO}$[c]	$(\Delta H^{\ddagger}_{is})_{exp}$[d]
Fe	0.04	0.33	0	0.02	1.14	1.17	0.3	0.25	0.2	1.7
Ni	5.60	5.55	1.4	1.4	16.30	21.35	5.7	4.6	2.2	1.9
Co	16.89	33.43	6.0	5.6	33.83	41.12	9.5	9.3	6.0	13.2

[a] Determined by the curve-crossing procedure illustrated in Figure 3. [b] Calculated from eq 3. [c] Calculated from eq 4. [d] Experimental value from Table 4 of ref 2.

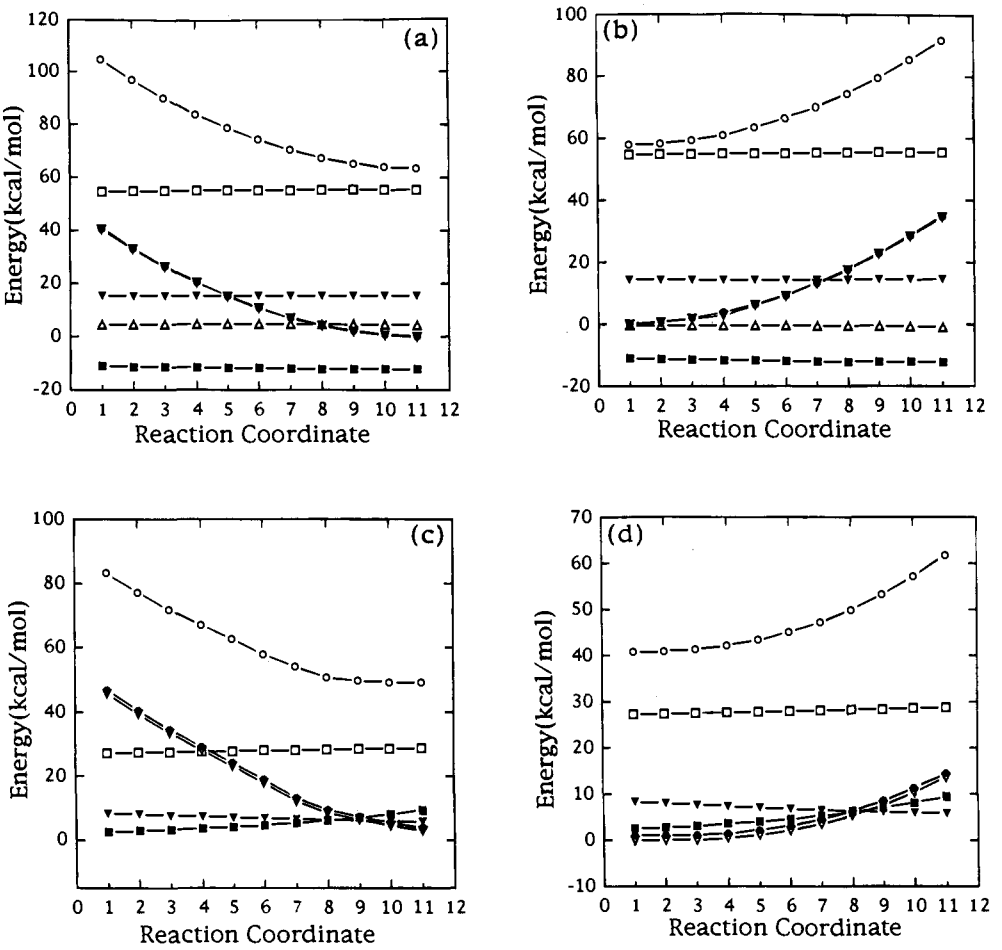

Figure 4. Contribution of component energy terms to total reorganization energy: (○) total; (●) stretching; (▼) bending; (□) torsion; (■) van der Waals; (△) electrostatic; (▽) stretching from 6 M−N bonds. (a) CHARMM using Co(tacn)$_2^{3+}$ force field, (b) CHARMM using Co(tacn)$_2^{2+}$ force field, (c) MMX using Co(tacn)$_2^{3+}$ force field, (d) MMX using Co(tacn)$_2^{2+}$ force field.

correspondence with one another for each computational method. This is not unexpected, because essentially harmonic motion is assumed for all reactants. Either quantity predicts the correct trend in $\Delta H^{\ddagger}_{is}$. However, computed values are uniformly smaller than $(\Delta H^{\ddagger}_{is})_{exp}$, with the exception of the Ni(tacn)$_2^{3+/2+}$ result from CHARMM. Also, it is interesting to note that the $(\Delta H^{\ddagger}_{is})_{MM}$ and $(\Delta H^{\ddagger}_{is})_{reorg}$ values obtained by MMX nearly equal those calculated by eq 4 $[(\Delta H^{\ddagger}_{is})_{HO}]$ employing $f_i = 1.70$ mdyn Å^{-1}, a commonly used value for the reduced force constant of M−N bonds in transition metal−amine complexes.[25] The numerical similarity between MMX results for k_s(M−N) in Table 2 and spectroscopically derived values of M−N stretching constants was noted earlier.

The correlation between $\Delta H^{\ddagger}_{is}$ values calculated by molecular mechanics (Table 6) and electron transfer rate constants (Table 1) is consistent with recent work of others who have employed computational methods to calculate inner-shell barriers to electron transfer in reactions characterized by large structural change. For example, Nelsen et al.[26] used semiempirical AM1 methods to support the observation that the neutral to cation oxidation of sesquibicyclic hydrazines is slow relative to other organic oxidations because of inner-shell effects. Evans et al.[27] investigated the inner-shell reorganizations attending electrochemical reduction of a series of α-methylated cycloalkane-1,2-diones also using AM1. Here, the correct sequence of reactivity was predicted, but differences in calculated $\Delta H^{\ddagger}$ values were not as large as suggested by ratios of measured electrochemical rate constants.

The inner-shell enthalpies of activation calculated for reaction 1 with M = Co are consistent with barriers of related homogeneous self-exchange reactions.[28] For example, the result $(\Delta H^{\ddagger}_{is})_{MM}$ = 6.0 kcal mol^{-1} calculated by MMX for Co(tacn)$_2^{3+/2+}$ is in close agreement with experimental values

(25) Sutin, N. *Prog. Inorg. Chem.* **1983**, *30*, 441.

(26) Nelsen, S. F.; Blackstock, S. C.; Kim, Y. *J. Am. Chem. Soc.* **1987**, *109*, 677.

(27) Brielbeck, B.; Rühl, J. C.; Evans, D. H. J. *Am. Chem. Soc.* **1993**, *115*, 11898.

(28) Activation enthalpies of homogeneous self-exchange reactions are divided by two in making comparisons with heterogeneous values.

of 5−7 kcal mol^{-1} reported for several $CoN_6^{3+/2}$ self-exchange reactions.[29] This figure is consistent also with inner-shell contributions of 6.9 and 4.5 kcal mol^{-1} calculated for $Co(en)_3^{3+/2}$ and $Co(sep)^{3+/2+}$, respectively, by Endicott et al.[29] using molecular mechanics and a value of 5.7 kcal mol^{-1} obtained for $Co(NH_3)_6^{3+/2}$ by Siders and Marcus[30] using classical, semiclassical, and quantum mechanical methods. Analogous comparisons are not possible for the Fe and Ni couples. However, the calculated values of $\Delta H^{\ddagger}_{is}$ for $Fe(tacn)_2^{3+/2+}$ in Table 6 appear to be rather small, and CHARMM computes a very large barrier for $Ni(tacn)_2^{3+/2+}$. The first discrepancy arises from the large uncertainty of the X-ray crystal structure data[5] used in the parametrization where little difference exists between the M−N bond distances of the $Fe(tacn)_2^{3+}$ and $Fe(tacn)_2^{2+}$ complexes. Hence, the difference between optimized Fe(III) and Fe(II) structures is small, and the uncertainty in reorganization energies derived from them is large. The origin of the large $Ni(tacn)_2^{3+/2+}$ barrier obtained from CHARMM appears to be the relatively large metal−nitrogen stretching force constant of the Ni(II) oxidation state (Table 2).

At present, there is no explanation for the discrepancy between calculated and experimental barrier heights. However, the electrode half-reaction entropies exhibit a significant metal dependence which is reproduced qualitatively by molecular mechanics calculations (Table 5). Experimental values of $\Delta H^{\ddagger}_{is}$ correlate with ΔS^0_{rc}.[2] The metal dependence of ΔS^0_{rc} is believed to arise from differences in the extent to which metal−ligand vibrational frequencies change with oxidation state.[24] This feature leads also to differences between $\lambda_{is,2}$ and $\lambda_{is,3}$. Although questions regarding the role of non-zero entropy differences on electron transfer reactivity have been addressed on several occasions,[31] it is not clear how this property might contribute to an increase in electrochemical activation barriers above their anticipated values. Further experimental and computational studies are needed to resolve this issue.

Internal Energy Distribution. An advantage of molecular mechanics is its ability to partition the total energy of a molecule into stretching, bending, torsional, and nonbonded components by means of the equations in the force field. We have done this employing the procedure whereby the inner-shell enthalpy of activation is estimated by distortion of ground state structures. Figure 4 presents the results of these calculations for $Co(tacn)_2^{3+/2+}$. As shown in Figure 4, and is true for the other complexes in this study, the dominant component of the total energy is the stretching term. This energy is a composite of all bond stretchings that occur in the transformation of $Co(tacn)_2^{3+}$ to $Co(tacn)_2^{2+}$; thus, the stretching contribution was further dissected into its individual components. The result is plotted as the ∇−∇ line in Figure 4 and shows that most of the stretching energy originates from deformation of the Co−N bonds and that relatively little derives from bonds in the remainder of the molecule. In addition, the energies of intraligand and interligand interactions are small. Endicott et al.[29] reached a similar conclusion regarding the Co−N deformations that accompany $Co(en)_3^{3+/2+}$ and $Co(sep)^{3+/2+}$ electron transfer.

The foregoing results also validate the frequent use of eq 4 as a means of estimating inner-shell reorganization energies. Metal−ligand linkages dominate this expression because they are the most deformable bonds in the molecule and thus experience the greatest structural change. Stretching, bending, and nonbonded interactions involving the ligand backbone atoms result in less structural change and do not contribute as much to the total difference in energy. In addition, we note that eq 4 treats metal−ligand deformation as a process controlled by a harmonic restoring force. The stretching potential in CHARMM also is harmonic in nature; therefore, M−N deformation energies calculated by this method should display the same characteristic. Since MMX accounts for anharmonic deformations and gives the same result as CHARMM, we deduce that an anharmonic description of M−N bond elongation is not required for the molecules in this study.

Acknowledgment. Support of this research by the National Science Foundation (CHE-9214784) is gratefully acknowledged. Y.-D.G. thanks Dr. Richard J. Loncharich of Lilly Research Laboratories for helpful discussions on computing. F.A.S. wishes to thank Professor R. A. Marcus for helpful conversation and Professor Fred C. Anson and the Division of Chemistry and Chemical Engineering at the California Institute of Technology for their hospitality during preparation of this manuscript.

JA950178Z

(29) Endicott, J. F.; Brubaker, G. R.; Ramasami, T.; Kumar, K.; Dwarakanath, K.; Cassel, J.; Johnson, D. *Inorg. Chem.* **1983**, *22*, 3754.

(30) Siders, P.; Marcus, R. A. *J. Am. Chem. Soc.* **1981**, *103*, 741.

(31) (a) Marcus, R. A.; Sutin, N. *Inorg. Chem.* **1975**, *14*, 213. (b) Hupp, J. T.; Weaver, M. J. *J. Phys. Chem.* **1984**, *88*, 6128. (c) Hupp, J. T.; Neyhart, G. A.; Meyer, T. J.; Kober, E. M. *J. Phys. Chem.* **1992**, *96*, 10820. (d) Weintraub, O.; Bixon, M. *J. Phys. Chem.* **1994**, *98*, 3407.